Modelling of a Charge Control Method for Capacitive MEMS

Panagiotis Giounanlis, Elena Blokhina and Orla Feely
School of Electrical, Electronic and Communications Engineering
University College Dublin
Dublin, Ireland

Manuel Domínguez, Joan Pons Nin and Sergi Gorreta
Micro and Nano Technologies group
Universitat Politècnica de Catalunya
Barcelona, Spain

***Abstract*—Charging of dielectric materials in microelectromechanical systems (MEMS) actuated electrostatically is a major reliability issue. In our previous work we proposed a feedback loop control method that is implemented as a circuit and that allows smart actuation for switches and varactors. In this paper we discuss system-level modeling of MEMS devices including all aspects of the system: proposed control method, charging dynamics and realistic models of the mechanical components of MEMS.**

I. Introduction

A variety of microelectromecanical systems including oscillators, variable capacitors (varactors) and switches are actuated electrostatically. Despite a number of advantages, this actuation technique may lead to the accumulation of charge in dielectric materials used for the fabrication of these MEMS. This is known to be a major reliability problem for these devices since the charge trapped in the dielectric causes a shift of the CV characteristic and even permanent stiction of movable mechanical parts to actuation electrodes. This is especially a problem for radio frequency (RF) MEMS [1]. As is reported in recent reviews [2], [3], the accumulation of charge by dielectrics is very common and all typical dielectric materials are prone to it. In recent years an alternative approach that consists of bipolar [4] and smart actuation techniques [5], [6] is suggested to address the problem of dielectric charging.

In ref. [6] we proposed a smart actuation method that is based on a feedback control. We have investigated this method for a simple 1D model suitable for MEMS positioners and varactors which operate below pull-in of the MEMS structure. (*Pull-in* is a phenomenon when a movable suspended electrode collapses onto the fixed electrode since the electrostatic force can no longer be compensated by the restoring mechanical force). In addition, we experimentally demonstrated that the method can be applied to switches which operate beyond pull-in. However the simplest model investigated in that paper does not include certain effects that can be found in realistic mechanical structures. It also does not allow us to apply the theory and numerical simulation technique to switches. The aim of this paper is to present a system level model that includes all aspects of the system: the charge control method which is implemented in a circuit, a realistic model of the mechanical part of the device and the dynamics of dielectric charging/discharging with time. The main advantage of the improved model that it allows simulations both below and beyond pull-in, i.e. it is suitable for modeling of varactors, positioners and switches. In addition, it is rather simple and has a form of a nonlinear discrete-time mapping. We also discuss how to extract the data of the dielectric charge from experiment and apply this model to simulate realistic devices used in experiment in [6].

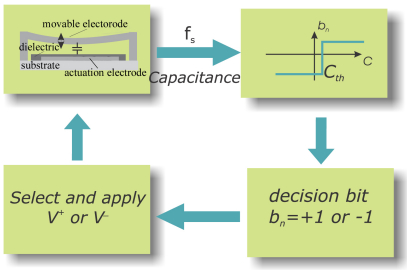

Fig. 1. Schematic block diagram of a charge control method. The capacitance of a microelectromechanical (MEM) structure is sampled, sensed and compared to the threshold value C_{th}. Based on this comparison, either a positive V^+ or a negative V^- actuation voltage is applied.

II. Statement of the Problem

A. Control Method for Dielectric Charge

The control method of dielectric charge, as shown in fig. 1, is based on the measurement of the capacitance of the device. As the capacitance of the device is related indirectly to the amount of the dielectric charge accumulated, at each time instant nT_s, the control method decides what voltage to apply for the next step $(n+1)T_s$ based on the state of the system. If Q_d is the accumulated dielectric charge, it causes the effective voltage be different from the actual applied voltage V:

$$V_{\text{eff}} = V - V_{\text{shift}}, \quad \text{where} \quad V_{\text{shift}} = \frac{Q_d}{Cd} \tag{1}$$

The general form of a discrete-time mapping that describes the control method from fig. 1 is given in [6] in the following form:

$$T(Q_d, b) = \begin{pmatrix} \Theta(P; Q_d, b) \\ \frac{1}{2}\left[1 + \text{sgn}\left(C_{th} - \frac{C_{g,0}}{1+\gamma - \mathcal{X}(V,Q_d)/g}\right)\right] \end{pmatrix} \tag{2}$$

where $T(Q_d, b)$ is an evolution operator which describes the charging dynamics, Q_d is the dielectric charge, b is a decision bit sequence (for more details see [6]), $\Theta(P; Q_d, b)$ is a function that expresses the evolution of the dielectric charge (see Sec. II-B) with P being the parameters of the charging model, C_{th} is a capacitance reference, $C_{g,0}$ is the initial capacitance of the device (when no voltage is applied), $\gamma = C_{g,0}/C_d$ with C_d the capacitance of the dielectric and

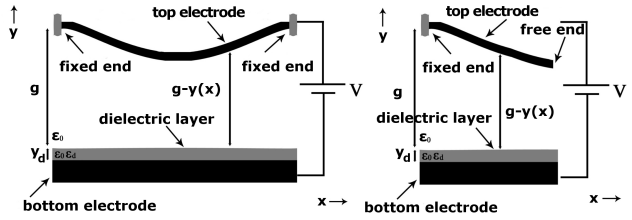

Fig. 2. Schematic view of a suspended bridge and a cantilever typically used as the mechanical structure in capacitive MEMS varactors and switches. In both cases, the applied voltage V causes the deflection of the beam and therefore a change in the capacitance of the device below and beyond pull-in.

$\mathcal{X}(V, Q_d)/g$ is a function of the position of the device for an applied voltage with g the gap distance. The control bit b denotes whether a positive V^+ ($b = +1$) or negative V^- ($b = -1$) voltage is applied.

Model (2) was originally suggested for 1D structures. The disadvantage of this 1D model is that it is unable to capture the dynamics of the system beyond the pull-in voltage. When the movable electrode collapses onto the bottom electrode, the capacitance of the devices in the 1D model is always equal to the capacitance of the dielectric C_d. In addition, this model is unable to fit experimental data that is an important step for the analysis of the charging/discharging dynamics. Therefore, a more realistic model is required.

We propose an improved model of the system in a very similar form:

$$T(Q_d, b) = \begin{pmatrix} \Theta(P; Q_d, b) \\ \frac{1}{2}\left[1 + \operatorname{sgn}\left(C_{th} - \mathcal{C}\left(y(x), V, Q_d\right)\right)\right] \end{pmatrix} \tag{3}$$

where $\mathcal{C}(y(x), V, Q_d)$ is a function representing a distributed capacitance of the device whose mechanical part has the form of continuous structure from fig. 2. Here the spatial distribution $y(x)$ is a function of the applied voltage V and the dielectric charge Q_d.

B. Charging and Discharging of the Dielectric: Dynamics

At this stage we have introduced the dielectric charge Q_d and linked it with the effective voltage V_{eff} given by (1). There are three most commonly used semi–empirical charging models that can be found in literature (see review given in [6] and also other works [7], [8]):

Model A (single exponential):
$$Q_d(t) = A_0 + A_1 \exp(-t/\tau)$$

Model B (multiple exponentials):
$$Q_d(t) = A_0 + \sum_n A_n \exp(-t_n/\tau_n)$$

Model C (stretched exponential):
$$Q_d(t) = A_0 + A_1 \exp\left[(-t/\tau)^\beta\right], \text{ where } 0 < \beta < 1$$

where the coefficients A_i and the characteristic times τ_i are to be determined from fitting of experiment data.

C. Improved Fitting of Experimental Data

In order to extract the realistic dynamics $Q_d(t)$ from experimental data, the following method is employed. In experiment, a capacitive MEMS devices was stressed by a constant voltage (either V^+ or V^-) over a long interval of time. The dielectric charge accumulates and causes the change of the effective voltage $V_{\text{eff}}(t)$ according to (1). The devices 'sees' this drift of $V_{\text{eff}}(t)$ and the capacitance of the device $C(t)$ also drifts with time. In a certain sense, a 'Capacitance-Voltage' characteristic $C(V_{\text{eff}})$ is indirectly measured in this experiment, though the exact change of $V_{\text{eff}}(t)$ is unknown and the aim of the fitting is to find it. However, with an improved mechanical model, we can calculate the analytical C-V curve for a device with known physical parameters for arbitrary range of the applied voltage. By comparing the experimental $C(V_{\text{eff}})$ and the analytical $C(V)$ we find what voltage causes the corresponding change in the capacitance. The charge now is $Q_d = [V_{\text{applied}} - V_{\text{analytical}}] \cdot C_d$. Figure 3 shows the result of the above fitting procedure for the experimental data for a MEMS device from [6]. The solid line shows the extracted experimental data $Q_d(t)$ and the other lines show interpolation of this data by the three different models.

III. Development of the Improved Model

Since we introduced the improved discrete-time mapping in the form (3), the function $\mathcal{C}(y(x), V, Q_d)$ and the distribution $y(x)$ must be defined and found. Below we describe how to find the distribution $y(x)$.

A. Discretization of the Governing Equation

The deflection of an elastic beam for a given applied voltage is described by the Euler–Bernoulli equation [9]:

$$\rho \frac{\partial^2 y}{\partial t^2} = -EI \frac{\partial^4 y}{\partial x^4} + F_{el} \tag{4}$$

where ρ is the density of the beam, E is the Young's Modulus, $I = bh^3/12$ is the moment of inertia, b is the width of the beam, h is the thickness of the beam and ℓ is the length of the beam. The force that acts on the beam

$$F_{el} = -\frac{1}{2} \frac{b\epsilon_0 V^2}{(g - y + \frac{y_d}{e_d})^2} \tag{5}$$

is an electrostatic force per unit of length. Here V is the applied voltage, ϵ_0 is the vacuum permittivity, ϵ_d is the relative permittivity of the dielectric, g is the gap distance between the up electrode and the dielectric and y_d is the thickness of the dielectric layer.

For a given voltage V, the beam will reach a steady-state distribution $y(x)$. The time required to reach it is very fast

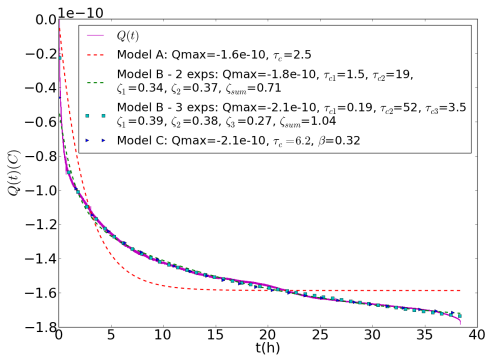

Fig. 3. Extraction and fitting of the experimental data $Q_d(t)$. Here ζ_i are the coefficients of exponentials and τ_{ci} are the characteristic time constants.

since the device operates in air. This allows us to neglect the time-dependent term in eq. (4). Therefore,

$$EI\frac{\partial^4 y}{\partial x^4} = F_{el} \tag{6}$$

Let us use the following normalized quantities [10]: $\hat{y} = y/g$, $\hat{x} = x/\ell$, $\hat{V} = \sqrt{(\epsilon_0 b\ell^4)/g^3}$, $\gamma = y_d/ge_d$ and $\hat{F_{el}} = \hat{V}^2/(2EI(1-\hat{y}+\gamma)^2)$. Considering the Taylor expression for the fourth-order derivative and introducing n discrete nodes in the beam domain we obtain a finite difference scheme for equation (6)

$$y_i = \frac{(\Delta x)^4}{6}\cdot(F_{el} + 4y_{i+1} + 4y_{i-1} - y_{i+2} - y_{i-2}) \tag{7}$$

where $\Delta x = \ell/(n-1)$ and $i = 1, 2, ..., n$. Here and later the "hat" symbols are omitted.

For the clamped–clamped beam shown in fig. 2a, both ends are fixed and the boundary conditions are [10]:

$$y(0) = y(\ell) = y'(0) = y'(\ell) = 0 \tag{8}$$

or equally if the variable $1-y$ is considered instead of y: $y(0) = y(\ell) = 1, \quad y'(0) = y'(\ell) = 0$.

For the cantilever beam, at the clamped end, the boundary conditions are the same as in previous case. For the free end, there are three cases described in [10]. The following one is used in this paper (a flat configuration):

$$y(0) = 1,\ y'(0) = 0,\ y(P) = 0,\ y'(P) = 0,\ y''(P) = 0 \tag{9}$$

where P is the point that separates the part of the beam which touches the bottom electrode from the part that has no contact with it. The corresponding finite differences scheme for a fixed end is

$$y_1 = 1, \quad y_{-1} - 8y_0 + 8y_2 - y_3 = 0 \tag{10}$$

The finite differences equations for the flat configuration are:

$$y_{n_p} = 0, \quad -y_{n_p+2} = 0 \tag{11}$$

$$-y_{n_p-2} + 2y_{n_p-1} - 2y_{n_p+1} + y_{n_p+2} = 0 \tag{12}$$

$$-y_{n_p-2} + 16y_{n_p-1} - 30y_{n_p} + 16y_{n_p+1} = 0 \tag{13}$$

where n_p is the first node in contact with the bottom electrode (all other nodes after this one are also in contact).

IV. Practical Implementation of the Model and Results

A. Modelling Below Pull-In

The regime below pull-in corresponds to MEMS varactors and positioners. In this case we expect that the improved model will give very similar results to the 1D model proposed in [6]. For applied voltages below the pull-in voltage, two techniques are proposed. The first technique, applicable to clamped–clamped system, uses an iterative method for equation (7) as described in [11]. The second technique, which is applicable for both clamped-clamped and cantilever systems, uses the Newton-Raphson algorithm to solve the system of $n+4$ nonlinear equations (7) together with the corresponding boundary conditions. Figure 4(a) compares the distribution of the beam for the same parameters and applied voltage calculated employing the two above techniques.

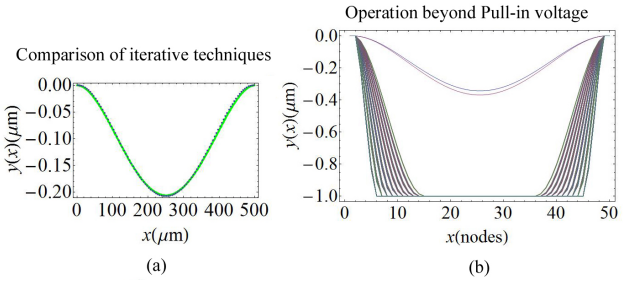

Fig. 4. (a) MEM clamped-clamped beam distribution along the axis x computed from two different techniques. The beam is discretized using 100 node for technique 1 (shown by dots) and 1000 nodes for technique 2 (shown by the solid line). (b) Evolution of the MEM beam distribution beyond pull in. The starting voltage is 15.1 V and the increment is 0.1 V.

Now the distribution $y(x)$ has been found. The function $\mathcal{C}(y(x), V, Q_d)$ is computed as the average of the expression $C_{g,0}/(1+\gamma-y_i/g)$ where y_i is the deflection of the i_{th} node of the beam. We can now apply the complete model (3) to calculate the performance of the device under the control method. Figure 5 shows the control method applied to a clamped-clamped MEM structure that models a variable capacitor. The results are very similar to those predicted by the 1D model in [6]. In simulations in this paper, we use the parameters given in Table I.

TABLE I
Parameters values

ℓ: $500\cdot10^{-6}m$	h: $4.3\cdot10^{-6}m$	b: $100\cdot10^{-6}m$	ϵ_d: 4
E: $1.3\cdot10^{11}Pa$	g: $10^{-6}m$	y_d: $85\cdot10^{-9}m$	

B. Modeling Beyond Pull-In

The regime beyond pull-in corresponds to MEMS switches. As in the previous case, there are two techniques that we can apply. The first approach is similar to those described in Sec. IV-A, however it has the following modification. If during the iterations the deflection of a node of the discretized beam is greater than or equal to the gap distance, it is set equal to the gap distance, and the iteration continues until the algorithm converges. The number of nodes whose deflection is equal to the gap distance corresponds to the fraction of the beam that is collapsed onto the bottom electrode. This approach

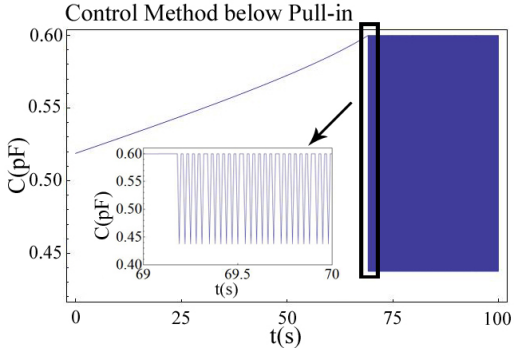

Fig. 5. The charge control method applied to a MEMS below pull-in. The capacitance as a function time and its magnified fragment are shown.

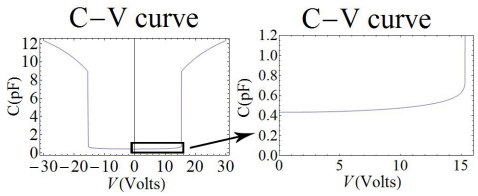

Fig. 6. Simulated C-V curve below and beyond pull-in for the parameters from Table I.

is applicable to clamped–clamped system. Figure 4(b) shows the evolution of the beam distribution if different voltages are applied. The starting voltage is 15.1 V (below pull-in) and the increment step is 0.1 V. After two steps, the graph visualizes the operation beyond pull-in. The number of nodes that have been used are $n = 50$.

In the second approach, by applying a voltage beyond pull-in we cause a part of the suspended electrode to collapse onto the bottom electrode. The part of the beam that is collapsed is the unknown and must be computed. The distribution of the beam is symmetrical on the right and left of this part. If the distribution of the beam that is not in contact with the bottom electrode on the left of the collapsed area is computed, the other half on the right has the same distribution. Let n_p be the first node that is collapsed. The number of this node is unknown, and in order to determine it, a shooting method is used.

For a given voltage and for a guessed number $n_{p,1}$, the system of nonlinear equations (7) together with the boundary conditions (11)-(13) for the right end is solved using the Newton-Raphson algorithm. The solution gives the distribution y_1. After, the second guess for $n_{p,2}$ is made, and the system of equations is solved again giving the new distribution y_2. Having the first two values, the new guess is extracted by using Newton's method for root finding. This repeats until boundary condition (10) is fulfilled with a required tolerance.

If $n_{p,0}$ is computed for a given voltage V_0, the value of n_p can then be calculated for any voltage V using the function $f(V) = n_{p_o} \cdot \frac{\sqrt{V_o}}{\sqrt{V}}$ [10]. This function will give real values for n_p, so these values must be rounded up and $n_p = \text{round}(n_{p_o} \cdot \frac{\sqrt{V_o}}{\sqrt{V}}) \in$ Integers. For a cantilever beam, a similar approach can be followed [10].

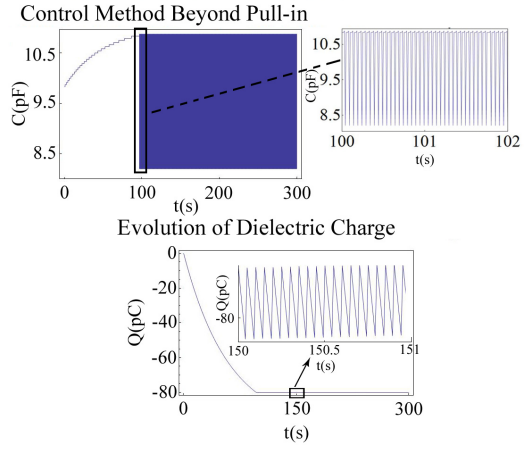

Fig. 7. Control method applied to a MEMS beyond pull-in. The capacitance as a function of time and its magnified fragment are shown on the top. The evolution of the dielectric charge with time is shown at the bottom. Model A as the charging dynamics is used with $Q_{\max} = -100$ pC, $\tau_C = \tau_D$ = 60 s. $V^+ = 18$ V and V^- = -17.5 V.

Implementing this approach, we can find the distribution of the mechanical structure for any given V beyond pull-in. Figure 6 shows the C-V curve of a MEMS device as computed for the parameters of Table I, including voltages below and beyond pull-in. Note that realistic MEM structures change their distributions even beyond pull-in, which cannot be predicted by the simple 1D model. This approach can be used together with the improved model (3) to find the capacitance function $\mathcal{C}(y(x))$. The control method applied to a structure beyond pull-in is shown in fig. 7 by the example of a clamped–clamped beam. This figure models the experimental example of a MEMS switch under the control method given in ref. [6].

V. Conclusions

In this paper we have developed system-level modeling of capacitive MEMS devices with a control method which is aimed at fixing the dielectric charge. In modeling, we include all aspects of the system: control method, charging dynamics and realistic models of the mechanical components of MEMS. We have shown that we can simulate the operation of MEMS both below and beyond pull-in voltages.

References

[1] E. S.Lucuszyn, "Advanced RF MEMS," *Cambridge, UK.: Cambridge Univ. Press*, 2010.

[2] W. M. van Spengen, "Capacitive RF MEMS switch dielectric charging and reliability: a critical review with recommendations," *Journal of Micromechanics and Microengineering*, vol. 22, no. 7, p. 074001, 2012.

[3] W. de Groot, J. Webster, D. Felnhofer, and E. Gusev, "Review of device and reliability physics of dielectrics in electrostatically driven MEMS devices," *Device and Materials Reliability, IEEE Transactions on*, vol. 9, no. 2, pp. 190 –202, june 2009.

[4] Z. Peng, X. Yuan, J. C. Hwang, D. I. Forehand, and C. L. Goldsmith, "Superposition model for dielectric charging of RF MEMS capacitive switches under bipolar control-voltage waveforms," *Microwave Theory and Techniques, IEEE Transactions on*, vol. 55, no. 12, pp. 2911–2918, 2007.

[5] T. Ikehashi, T. Miyazaki, H. Yamazaki, A. Suzuki, E. Ogawa, S. Miyano, T. Saito, T. Ohguro, T. Miyagi, Y. Sugizaki, N. Otsuka, H. Shibata, and Y. Toyoshima, "An RF MEMS variable capacitor with intelligent bipolar actuation," in *Solid-State Circuits Conference, 2008. ISSCC 2008. Digest of Technical Papers. IEEE International*, Feb., pp. 582–637.

[6] E. Blokhina, S. Gorreta, D. Lopez, D. Molinero, O. Feely, J. Pons-Nin, and M. Dominguez-Pumar, "Dielectric charge control in electrostatic MEMS positioners/varactors," *Microelectromechanical Systems, Journal of*, vol. 21, no. 3, pp. 559 –573, June 2012.

[7] S. Kalicinski, M. Wevers, and I. D. Wolf, "Charging and discharging phenomena in electrostatically-driven single-crystal-silicon MEM resonators: DC bias dependence and influence on the series resonance frequency," *Microelectronics Reliability*, vol. 48, pp. 1221 – 1226, 2008, 19th European Symposium on Reliability of Electron Devices, Failure Physics and Analysis (ESREF 2008).

[8] X. Yuan, Z. Peng, J. Hwang, D. Forehand, and C. Goldsmith, "A transient SPICE model for dielectric-charging effects in RF MEMS capacitive switches," *Electron Devices, IEEE Transactions on*, vol. 53, no. 10, pp. 2640 –2648, oct. 2006.

[9] D. J. IJntema and H. A. Tilmans, "Static and dynamic aspects of an air gap capacitor," *Sensors and Actuators A: Physical*, vol. 35, no. 2, pp. 121–128, 1992.

[10] S. Gorthi, A. Mohanty, and A. Chatterjee, "Cantilever beam electrostatic MEMS actuators beyond pull-in," *Journal of Micromechanics and MicroEngineering*, vol. 16, no. 9, pp. 1800–1810, 2006.

[11] A. Jain, S. Palit, and M. Alam, "A physics-based predictive modeling framework for dielectric charging and creep in RF MEMS capacitive switches and varactors," *Microelectromechanical Systems, Journal of*, vol. 21, no. 2, pp. 420 –430, april 2012.